DESIGNING AN ADAPTIVE CONTROLLER FOR TWO-WHEELED SELF-BALANCING MOBILE ROBOT USING HIERARCHICAL SLIDING CONTROL STRATEGY AND RADIAL BASIS FUNCTION NEURAL NETWORK

THIẾT KẾ BỘ ĐIỀU KHIỂN THÍCH NGHI CHO ROBOT HAI BÁNH TỰ CÂN BẰNG
SỬ DỤNG CHIẾN LƯỢC ĐIỀU KHIỂN TRƯỢT TẦNG VÀ MẠNG NƠRON RBF

Hoang Thi Tu Uyen[1], Kim Dinh Thai[2],
Pham Viet Anh[2], Dinh Xuan Minh[3], Le Xuan Hai[2,*]

ABSTRACT

This paper presents a novel adaptive controller for two-wheeled self-balancing mobile robots combining sliding mode control and hierarchical sliding control techniques. In addition, the radial basis function neural networks (RBFNN) are also applied to approximate the uncertain components in the system. The stability of the closed-loop control system is proven based on the Lyapunov principle. The simulation results show that the proposed controller's response quality is excellent even if the system is affected by unexpected external disturbances.

Keywords: Two-wheeled self-balancing mobile robot, Sliding mode control, Hierarchical sliding control, Radial basis function neural network.

TÓM TẮT

Bài báo này trình bày về một bộ điều khiển thích nghi mới cho robot hai bánh tự cân bằng bằng việc kết hợp những kỹ thuật điều khiển trượt và điều khiển trượt tầng. Bên cạnh đó, mạng nơ ron RBF cũng được sử dụng để xấp xỉ các thành phận phi tuyến trong hệ thống. Tính ổn định của hệ thống điều khiển vòng kín được chứng minh dựa theo nguyên lý Lyapunov. Những kết quả mô phỏng cho thấy chất lượng đáp ứng của bộ điều khiển để xuất là rất tốt ngay cả khi hệ thống chịu ảnh hưởng bởi nhiễu ngoài không biết trước.

Từ khóa: Xe hai bánh tự cân bằng, điều khiển trượt, điều khiển trượt tầng, mạng nơ ron RBF.

[1]Faculty of Automation, Industrial University of Ho Chi Minh City
[2]HaUI Institute of Technology, Ha Noi University of Industry
[3]Faculty of Electrical Engineering, Hanoi University of Industry
*Email: hailx@haui.edu.vn

1. INTRODUCTION

A two-wheeled self-balancing mobile robot (TWSBMR) or two-wheeled inverted pendulum robot is a naturally unstable system that comprises a two-wheel chassis and an inverted pendulum body. Despite the inverted pendulum structure of the TWSBMR causing postural instability, it provides many benefits for driving efficiency. In contrast to a three-wheeler or a four-wheeler, it can pass through narrow spaces and allows the driver to maintain an upright posture on inclined terrains and steer on the spot. As a result, TWSBMR is widely used in practical applications, such as unmanned navigation vehicles [1-3], personal transporters [4, 5], wheeled humanoids [6], and robot wheelchairs for the disabled [7, 8].

The TWSBMR is characterized by highly nonlinear and inherently unstable dynamics and is classified as an underactuated system [9]. With just two actuator inputs of both wheels, it implements three movements: pitch, yaw, and forward. Therefore, controlling a robot to move as desired while maintaining upright posture is a challenging topic that has drawn the attention of researchers around the world [9]. Similar to other underactuated systems, control methods for TWSBMR are diverse, ranging from simple linear control techniques to complex nonlinear control techniques. Several studies based on linear control techniques for TWSBMR have been reported in the literature, such as PID control [10-12], pole placement [13, 14], and linear quadratic regulator (LQR) [15, 16]. However, linear control approaches cannot maintain postural stability as soon as the TWSBMR enters a zone of nonlinear behavior with large pitch angles due to intentional maneuvers or external disturbances [17]. Many nonlinear control methods have been developed to address this issue, such as feedback linearization [18, 19], model predictive control (MPC) [20, 21], and sliding mode control (SMC) [22-24], fuzzy control [25-29], neuro-adaptive control [30-33]. Consequently, nonlinear control approaches remain favored and more efficient for TWSBMR control.

Among the nonlinear control methods, the SMC scheme is an excellent candidate for controlling underactuated, nonlinear systems. SMC is designed in two steps. First, design an appropriate sliding surface that determines the system's behavior during sliding. Subsequently, a control action is designed to lead all state trajectories to the sliding surface in finite-time and then force them to remain there. Once trajectories are established on the sliding surface, the system becomes insensitive to modeling errors and external disturbances. There have been some other variations based on the SMC scheme to design a controller for TWSBMR, such as discrete-time SMC [34, 35], higher-order SMC [36]. For instance, H. Aithal and S. Janardhanan [36] have proposed a second-order SMC method for trajectory tracking of a two-wheeled mobile robot. Although this approach has the advantage of eliminating chattering, it is computationally heavy compared to conventional SMC and requires prior knowledge of system parameters.

In this paper, we present a novel control method for TWSBMR, named adaptive hierarchical sliding mode control (AHSMC), combining SMC, hierarchical SMC (HSMC) and radial basis function neural networks (RBFNN). The HSMC technique is used in this study since it is well suited to underactuated systems and is also highly sustainable [37]. First, the controller is designed based on SMC and HSMC techniques, abbreviated as HSMC, to stabilize the system states on the sliding surface. The RBF neural network is then employed to approximate TWSBMR's uncertainty components. The RBF network is used here because it can approximate any nonlinear function with arbitrary precision when hidden layer nodes are large enough [38]. Moreover, it has a simple structure with only one input layer, one hidden layer and one output layer, and it is very suitable for real-time applications. As a result, the proposed controller is robust against parametric uncertainties and external disturbances, allowing fast convergence and high tracking accuracy.

The remainder of the paper is organized as follows: Section 2 presents the dynamic model of the system, while the control design steps are introduced in Section 3; Section 4 provides simulation results, and some concluding remarks are drawn in Section V.

2. DYNAMIC MODEL

It is necessary to build a dynamic model of the system before designing the controller for TWSBMR. A reliable dynamic model is a prerequisite for any model-based control design. This study uses the TWSBMR mathematical model as detailed in [39], which is built from the Euler-Lagrange equation.

The TWSBMR comprises three rigid bodies, two wheels on either side and an inverted pendulum, as shown in Fig. 1. In the fixed coordinate system {N}, x denotes the robot's displacement in straight motions, ψ denotes the robot's rotation angle in yaw motions, and θ denotes the body's tilt

angle in pitch motions. Hence, TWSBMR's motion is characterized by the state vector $q = \begin{bmatrix} x & \theta & \psi \end{bmatrix}^T$.
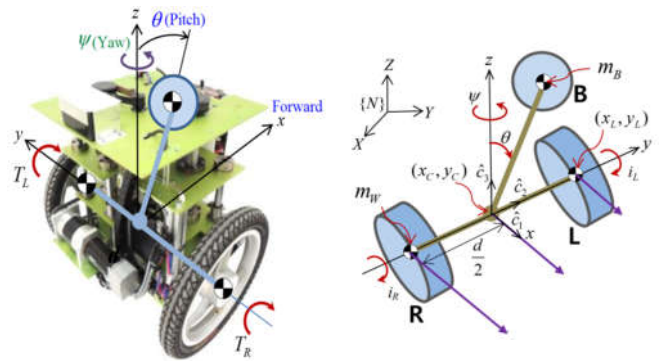
Figure 1. Schematic of the two-wheeled self-balancing mobile robot

The relationship between a wheel's torque and the current flowing through it is described as follows

$$\begin{cases} T_L = K_m i_L \\ T_R = K_m i_R \end{cases} \quad (1)$$

where T_L, T_R, i_L, i_R is the torque, the electric current of the left and right wheel, respectively.

With model parameters as listed in Table 1, TWSBMR's equation of motion is as follows

$$M\ddot{q} + (C + D)\dot{q} + G = B\tau \quad (2)$$

where $M, C, D \in \mathbb{R}^{3 \times 3}$ is the inertia matrix, centrifugal and Coriolis force matrix, damping matrix, respectively. $G \in \mathbb{R}^{3 \times 1}$ is the gravity matrix, $B \in \mathbb{R}^{3 \times 2}$ is the input transformation matrix, and $\tau = \begin{bmatrix} i_L & i_R \end{bmatrix}^T$ is the input matrix.

$$M = M(q) = \begin{bmatrix} m_{11} & m_{12} & 0 \\ m_{21} & m_{22} & 0 \\ 0 & 0 & m_{33} \end{bmatrix},$$

$$C = C(q, \dot{q}) = \begin{bmatrix} 0 & c_{12} & c_{13} \\ 0 & 0 & c_{23} \\ c_{31} & c_{32} & c_{33} \end{bmatrix},$$

$$D = \begin{bmatrix} d_{11} & d_{12} & 0 \\ d_{21} & d_{22} & 0 \\ 0 & 0 & d_{33} \end{bmatrix}, G = G(q) = \begin{bmatrix} 0 \\ -m_B gl\sin\theta \\ 0 \end{bmatrix},$$

$$B = \begin{bmatrix} \dfrac{K_m}{r} & \dfrac{K_m}{r} \\ -K_m & -K_m \\ \dfrac{-K_m d}{2r} & \dfrac{K_m d}{2r} \end{bmatrix}$$

The elements of the matrices M, C, D are as follows

$$m_{11} = m_B + 2m_W + \frac{2J}{r^2}, m_{12} = m_{21} = m_B l\cos\theta, m_{22} = I_2 + m_B l^2$$

$$m_{33} = I_3 + 2K + \left(m_W + \frac{J}{r^2}\right)\frac{d^2}{2} - \left(I_3 - I_1 - m_B l^2\right)\sin^2\theta$$

$$c_{12} = -m_B l\dot{\theta}\sin\theta \,, \ c_{13} = -m_B l\dot{\psi}\sin\theta \,,$$

$$c_{23} = \left(I_3 - I_1 - m_B l^2\right)\dot{\psi}\sin\theta\cos\theta$$

$$c_{31} = m_B l\dot{\psi}\sin\theta \,, \ c_{32} = -\left(I_3 - I_1 - m_B l^2\right)\dot{\psi}\sin\theta\cos\theta \,,$$

$$c_{33} = -\left(I_3 - I_1 - m_B l^2\right)\dot{\theta}\sin\theta\cos\theta$$

$$d_{11} = \frac{2c_\alpha}{r^2} \,, \ d_{12} = d_{21} = \frac{-2c_\alpha}{r} \,, \ d_{22} = 2c_\alpha \,, \ d_{33} = \frac{d^2 c_\alpha}{2r^2}$$

Table 1. Model parameters of TWSBMR

Symbol	Definition
d	Distance between the two wheels
l	Length of pendulum
r	Radius of wheels
m_B	Mass of the pendulum body (except wheels)
m_W	Mass of each wheel
J, K	Mass moment of inertia (MOI) of each wheel w.r.t. the wheel axis and the vertical axis.
I_1, I_2, I_3	MOI of the pendulum body w.r.t.

From (2), it is deduced that

$$\begin{bmatrix} \ddot{x} \\ \ddot{\theta} \\ \ddot{\psi} \end{bmatrix} = \begin{bmatrix} f_1 \\ f_2 \\ f_3 \end{bmatrix} + \begin{bmatrix} -b_1 & -b_1 \\ b_2 & b_2 \\ c_1 & -c_1 \end{bmatrix} \begin{bmatrix} i_R \\ i_L \end{bmatrix} \tag{3}$$

where $b_1 = \dfrac{\left(m_{12} + \dfrac{m_{22}}{r}\right)K_m}{m_{12}m_{21} - m_{11}m_{22}}$, $b_2 = \dfrac{\left(m_{11} + \dfrac{m_{21}}{r}\right)K_m}{m_{12}m_{21} - m_{11}m_{22}}$,

$$c_1 = \frac{K_m d}{2ra_{33}},$$

$$f_1 = \frac{\begin{aligned}&\left(m_{22}d_{11} - m_{12}d_{21}\right)\dot{x} + \left[\left(c_{12} + d_{12}\right)m_{22} - m_{12}d_{22}\right]\dot{\theta} \\ &+ \left(m_{22}c_{13} - m_{12}c_{23}\right)\dot{\psi} + m_{12}m_B gl\sin\theta\end{aligned}}{m_{12}m_{21} - m_{11}m_{22}}$$

$$f_2 = \frac{\begin{aligned}&\left(m_{21}d_{11} - m_{21}m_{11}\right)\dot{x} + \left[\left(c_{12} + d_{12}\right)m_{21} - d_{22}\right]\dot{\theta} \\ &+ \left(m_{11}c_{23} - m_{21}c_{13}\right)\dot{\psi} - m_{11}m_B gl\sin\theta\end{aligned}}{m_{12}m_{21} - m_{11}m_{22}}$$

$$f_3 = -\frac{c_{31}\dot{x} + c_{32}\dot{\theta} + \left(c_{33} + d_{33}\right)\dot{\psi}}{m_{33}}$$

3. CONTROLLER DESIGN

Let us define

$$x = \begin{bmatrix} x_1 & x_2 & x_3 & x_4 & x_5 & x_6 \end{bmatrix}^T = \begin{bmatrix} x & \dot{x} & \theta & \dot{\theta} & \psi & \dot{\psi} \end{bmatrix}^T$$

Two virtual control signals are defined as follows

$$\begin{cases} u_1 = i_L + i_R \\ u_2 = i_R - i_L \end{cases} \tag{4}$$

Then, Eq. (3) is rewritten as follows

$$\begin{cases} \dot{x}_1 = x_2 \\ \dot{x}_2 = f_1 + g_1 u_1 \\ \dot{x}_3 = x_4 \\ \dot{x}_4 = f_2 + g_2 u_1 \\ \dot{x}_5 = x_6 \\ \dot{x}_6 = f_3 + g_3 u_2 \end{cases} \tag{5}$$

Definition of tracking errors

$$e_1 = x_1 - x_d = x - x_d; e_2 = \dot{e}_1$$

$$e_3 = x_4 - \theta_d = \theta - \theta_d; e_4 = \dot{e}_3$$

$$e_5 = x_5 - \psi_d = \psi - \psi_d; e_6 = \dot{e}_5$$

Where x_d, θ_d, ψ_d are the reference values of x, θ and ψ, respectively.

Hence, Eq. (5) is rewritten in error form as follows

$$\begin{cases} \dot{e}_1 = e_2 \\ \dot{e}_2 = f_1 + g_1 u_1 - \ddot{x}_d \\ \dot{e}_3 = e_4 \\ \dot{e}_4 = f_2 + g_2 u_1 - \ddot{\theta}_d \\ \dot{e}_5 = e_6 \\ \dot{e}_6 = f_3 + g_3 u_2 = \ddot{\psi}_d \end{cases} \tag{6}$$

3.1. Hierarchical sliding mode controller design

This section applies the hierarchical sliding mode control strategy [37] to design a controller that stabilizes forward and pitch movements.

Step 1: Considerring the first subsystem in (6)

$$\begin{cases} \dot{e}_1 = e_2 \\ \dot{e}_2 = f_1 + g_1 u_{11} - \ddot{x}_d \end{cases} \tag{7}$$

where u_{11} is the virtual control signal to ensure this subsystem is stable, i.e. $\lim\limits_{t \to \infty} e_1 = 0$

The first-level sliding surface for first subsystem is defined as

$$s_1 = c_1 e_1 + e_2 \tag{8}$$

where c_1 is arbitrary positive constant.

The control law for (7) consists of two components, the equivalent control law and switching control law, which are designed as follows:

$$u_{11} = u_{11eq} + u_{11sw} \tag{9}$$

$$\begin{cases} u_{11eq} = -\dfrac{c_1 e_2 + f_1}{g_1} \\ u_{11sw} = -\dfrac{k_1 s_1 + \eta_1 \text{sign}(s_1) - \ddot{x}_d}{g_1} \end{cases} \tag{10}$$

where k_1, η_1 are arbitrary positive constants.

Differentiating s_1 with respect to time yields

$$\dot{s}_1 = c_1e_2 + f_1 + g_1(u_{11eq} + u_{11sw}) - \ddot{x}_d$$
$$= (c_1e_2 + f_1 + g_1u_{11eq}) + (g_1u_{11sw} - \ddot{x}_d)$$
$$= -k_1s_1 - \eta_1 sign(s_1)$$

Considering the following Lyapunov function as follows:

$$V_1 = \frac{1}{2}s_1^2$$

Differentiating V_1 with respect to time yields

$$\dot{V}_1 = s_1\dot{s}_1 = -k_1s_1^2 - \eta_1s_1 sign(s_1) \leq 0$$

Thus, s_1 is stable according to the Lyapunov criterion, i.e. $\lim_{t\to\infty} s_1 = 0$. According to the definition of the sliding surface, the state error $\lim_{t\to\infty} e_1 = 0$.

Step 2: Considerring the second subsystem in (6):

$$\begin{cases} \dot{e}_3 = e_4 \\ \dot{e}_4 = f_2 + g_2u_{12} - \ddot{\theta}_d \end{cases} \quad (11)$$

The first-level sliding surface for second subsystem is defined as:

$$s_2 = c_2e_3 + e_4 \quad (12)$$

where c_2 is arbitrary positive constant.

The control law for (11) consists of two components, the equivalent control law and switching control law, which are designed as follows:

$$u_{12} = u_{12eq} + u_{12sw} \quad (13)$$

$$u_{12eq} = -\frac{c_2e_4 + f_2}{g_2} \quad (14)$$

Step 3: Considerring first and second subsystem in (6)

$$\begin{cases} \dot{e}_1 = e_2 \\ \dot{e}_2 = f_1 + g_1u_1 - \ddot{x}_d \\ \dot{e}_3 = e_4 \\ \dot{e}_4 = f_2 + g_2u_1 - \ddot{\theta}_d \end{cases} \quad (15)$$

The second-level sliding surface for two subsystems is defined as:

$$S = \lambda_1s_1 + \beta_1s_2 = \lambda_1(c_2e_1 + e_2) + \beta_1(c_2e_3 + e_4) \quad (16)$$

where λ_1, β_1 are arbitrary positive constants.

Differentiating S with respect to time yields

$$\dot{S} = \lambda_1\dot{s}_1 + \beta_1\dot{s}_2 = \lambda_1(c_2\dot{e}_1 + \dot{e}_2) + \beta_1(c_2\dot{e}_3 + \dot{e}_4)$$
$$= \lambda_1c_2e_2 + \beta_1c_2e_4 + \lambda_1(f_1 + g_1u_1 - \ddot{x}_d) + \beta_1(f_2 + g_2u_1 - \ddot{\theta}_d) \quad (17)$$

Let us consider the following Lyapunov function as:

$$V = \frac{1}{2}S^2 \quad (18)$$

Differentiating both sides of (18) with respect to time yields

$$\dot{V} = S * \dot{S} \quad (19)$$

where k_2, η_2 are arbitrary positive constants.

The common control signal (u_1) for the first and second subsystem in (33) is defined as:

$$u_1 = u_{11eq} + u_{11sw} + u_{12eq} + u_{12sw} \quad (20)$$

Substituting (28), (29) and (34) into (33) and simplifying yields

$$\dot{S} = \begin{pmatrix} (\lambda_1g_1 + \beta_1g_2)(u_{11sw} + u_{12sw}) + \\ \beta_1g_2u_{11eq} + \lambda_1g_1u_{12eq} - \lambda_1\ddot{x}_d - \beta_1\ddot{\theta}_d \end{pmatrix} \quad (21)$$
$$= -k_2S - \eta_2 sign(S)$$

The control signals u_{11sw}, u_{12sw} are designed so that

$$u_{12sw} + u_{11sw} = -\frac{\lambda_1g_1u_{12eq} + \beta_1g_2u_{11eq}}{\lambda_1g_1 + \beta_1g_2}$$
$$-\frac{k_2S + \eta_2 sign(S) - \lambda_1\ddot{x}_d - \beta_1\ddot{\theta}_d}{\lambda_1g_1 + \beta_1g_2} \quad (22)$$

Then,

$$\dot{V} = S * \dot{S} = -k_2S^2 - \eta_2|S| \leq 0 \quad (23)$$

Substituting (10), (14) and (22) into (20), we derive the control signal for the first two subsystems in (33) as follows:

$$u_1 = -\frac{\lambda_1f_1 + \beta_1f_2 + \lambda_1c_1e_2 + \beta_1c_2e_4}{\lambda_1g_1 + \beta_1g_2}$$
$$-\frac{k_2S + \eta_2 sign(S) - \lambda_1\ddot{x}_d - \beta_1\ddot{\theta}_d}{\lambda_1g_1 + \beta_1g_2} \quad (24)$$

3.2. Sliding mode controller design

Considerring the 3rd subsystem in (6):

$$\begin{cases} \dot{e}_5 = e_6 \\ \dot{e}_6 = f_3 + g_3u_2 \end{cases} \quad (25)$$

The sliding surface for this subsystem is defined as:

$$s_3 = e_6 + c_3e_5 \quad (26)$$

where c_3 is a arbitrary positive constant.

Taking the derivative of s_3 with respect to time yields

$$\dot{s}_3 = f_3 + g_3u_2 - \ddot{\psi}_d + c_3e_6 \quad (27)$$

Using a Lyapunov candidate function as follows:

$$V_3 = \frac{1}{2}s_3^2 \quad (28)$$

Differentiating both sides of (28) with respect to time yields

$$\dot{V}_3 = s_3\dot{s}_3 = s_3(f_3 + g_3u_2 - \ddot{\psi}_d + c_3e_6)$$

The control signal for (25) is defined as:

$$u_2 = g_3^{-1}(-f_3 + \ddot{\psi}_d - c_3e_6 - k_3 sign(s_3) - \eta_3s_3) \quad (29)$$

where k_3, η_3 are arbitrary positive constants.

Then $\dot{V}_3 = -k_3 s_3^2 - \eta_3 |s_3| \leq 0$.

Thus, s_3 is stable according to the Lyapunov criterion, i.e. $\lim\limits_{t\to\infty} s_3 = 0$ and $\lim\limits_{t\to\infty} e_5 = 0$

For reducing chattering at high frequencies, the sign(.) function in (24), (29) is replaced by a sat(.) function defined as follows:

$$\text{sat}(x) = \begin{cases} \text{sign}(x), & |x| > 1 \\ x, & |x| \leq 1 \end{cases} \tag{30}$$

By substituting the virtual control signals u_1, u_2 provided in (24), (29) into (4), we determine the corresponding current signals for the TWSBMR's wheel motors.

3.3. Adaptive rule design

Considering the dynamic model of TWSBMR in (27): the matrices C, D, G contain uncertain components that are difficult to determine in practice. Additionally, the functions f_1, f_2, f_3 in (32) contain the elements of these matrices. Therefore, SMC and HSMC controllers designed in the previous section are unlikely to achieve high accuracy in actual TWSBMR control. As a result, to increase the robustness of HSMC and SMC controllers with model uncertainty and the effects of unknown external disturbances, this section proposes an AHSMC controller using RBF neural network (RBFNN) [38] for adaptively estimation the functions f_1, f_2, f_3.
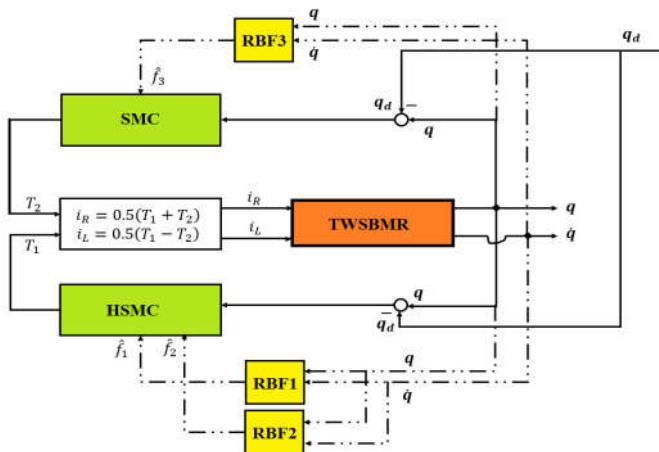
Figure 2. Proposed TWSBMR control structure diagram
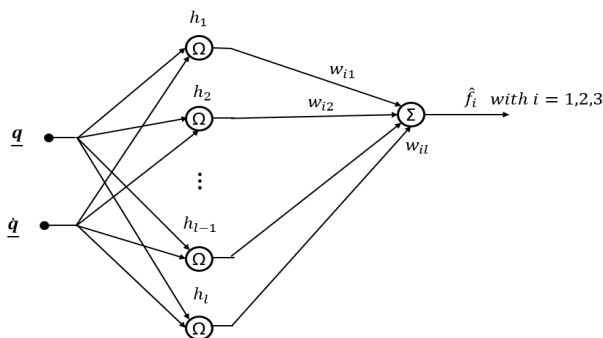
Figure 3. RBF neural network structure for approximating functions f_1, f_2, f_3

Fig. 2 shows the proposed TWSBMR control structure diagram, in which the three networks RBF1, RBF2 and RBF3 are RBFNNs used to approximate functions f_1, f_2, f_3 respectively. These networks have the same structure, as depicted in Fig. 3. The RBFNN's inputs include a position vector $q = \begin{bmatrix} x & \theta & \psi \end{bmatrix}^T$ and a velocity vector $\dot{q} = \begin{bmatrix} \dot{x} & \dot{\theta} & \dot{\psi} \end{bmatrix}^T$.

The output of the RBF1, RBF2 and RBF3 networks denoted $\hat{f}_1, \hat{f}_2, \hat{f}_3$, are approximations of f_1, f_2, f_3, respectively. The RBFNN's hidden layer includes l nodes $h = \begin{bmatrix} h_1 & h_2 & \cdots & h_l \end{bmatrix}^T$, defined as follows:

$$h_i = \frac{\exp\left(-\dfrac{\langle q - \underline{c}_{1i}, q - \underline{c}_{1i} \rangle + \langle \dot{q} - \underline{c}_{2i}, \dot{q} - \underline{c}_{2i} \rangle}{b_i^2}\right)}{\sum\limits_{j=1}^{l} \exp\left(-\dfrac{\langle q - \underline{c}_{1j}, q - \underline{c}_{1j} \rangle + \langle \dot{q} - \underline{c}_{2j}, \dot{q} - \underline{c}_{2j} \rangle}{b_j^2}\right)}, \, i=1,2,\ldots,l. \tag{31}$$

where $\langle .,. \rangle$ is the scalar product operator defined in normed space $\langle \mathbb{R}^n, \|.\| \rangle$.

It is noted that with sufficient nodes in the hidden layer (l), an RBF neural network can approximate any nonlinear function with arbitrary precision.

As a result, the RBF1, BRF2 and RBF3's outputs are presented as follows:

$$\begin{cases} f_1 = W_1^T h + \varepsilon_1 \\ f_2 = W_2^T h + \varepsilon_2 \\ f_3 = W_3^T h + \varepsilon_3 \end{cases} \tag{32}$$

where ε_1, ε_2, ε_3 are minor errors, $W_i = \begin{bmatrix} w_{i1} & w_{i2} & \cdots & w_{il} \end{bmatrix}^T$ with i = 1, 2, 3 is the ideal weights vector between the hidden and the output layer.

Let $\hat{W}_1, \hat{W}_2, \hat{W}_3$ denote estimations of W_1, W_2, W_3 respectively.

$$\begin{cases} \hat{f}_1 = \hat{W}_1^T h \\ \hat{f}_2 = \hat{W}_2^T h \\ \hat{f}_3 = \hat{W}_3^T h \end{cases} \tag{33}$$

The estimation errors for W_1, W_2, W_3 are determined as:

$$\begin{cases} \tilde{W}_1 = W_1 - \hat{W}_1 \\ \tilde{W}_2 = W_2 - \hat{W}_2 \\ \tilde{W}_3 = W_3 - \hat{W}_3 \end{cases} \tag{34}$$

The control signals in (47) and (50) are rewritten as follows:

$$\hat{u}_1 = -\frac{\lambda_1 \hat{f}_1 + \beta_1 \hat{f}_2 + \lambda_1 c_1 e_2 + \beta_1 c_2 e_4}{\lambda_1 g_1 + \beta_1 g_2} - \frac{k_2 S + \eta_2 \text{sat}(S) - \lambda_1 \ddot{x}_d - \beta_1 \ddot{\theta}_d}{\lambda_1 g_1 + \beta_1 g_2} \tag{35}$$

$$\hat{u}_2 = g_3^{-1}\left(-\hat{f}_3 + \ddot{\psi}_d - c_3 e_6 - k_3 sat(s_3) - \eta_3 s_3\right) \quad (36)$$

Theorem: An updated law for neural network's weight matrices are selected as follows:

$$\begin{cases} \dot{\hat{W}}_1 = -\dot{\tilde{W}}_1 = F_1\left(\lambda_1 Sh - \alpha\|S\|\hat{W}_1\right) \\ \dot{\hat{W}}_2 = -\dot{\tilde{W}}_2 = F_2\left(\beta_1 Sh - \alpha\|S\|\hat{W}_2\right) \\ \dot{\hat{W}}_3 = -\dot{\tilde{W}}_3 = F_3\left(sh - \alpha\|s_3\|\hat{W}_3\right) \end{cases} \quad (37)$$

where F_1, F_2, F_3 and α, σ are preselected positive constants.

If the following conditions are satisfied

$$\begin{cases} \|S\| > \dfrac{\varepsilon_{N1}}{k_2} + \alpha\dfrac{\|W_1\|_F^2 + \|W_2\|_F^2}{4k_2} \\ \|s_3\| > \dfrac{\varepsilon_{N2}}{\eta_3} + \sigma\dfrac{\|W_3\|_F^2}{4\eta_3} \end{cases} \quad (38)$$

where $\varepsilon_{N1} = \|\lambda_1\varepsilon_1 + \beta_1\varepsilon_2\|$, $\varepsilon_{N2} = \|\varepsilon_3\|$ then the closed-loop system will be stable according to Lyapunov criterion.

Proof:

Considerring the Lyapunov function in quadratic form as follows:

$$V = \frac{1}{2}S^2 + \frac{1}{2}tr\left(\tilde{W}_1^T F_1^{-1}\tilde{W}_1\right) + \frac{1}{2}tr\left(\tilde{W}_2^T F_2^{-1}\tilde{W}_2\right) \quad (39)$$

Here, the matrix trace operator tr(X) is defined as the sum of all the elements along the main diagonal of matrix X.

Taking the derivative of both sides of (39) with respect to time yields

$$\dot{V} = S\dot{S} + tr\left(\tilde{W}_1^T F_1^{-1}\dot{\tilde{W}}_1\right) + tr\left(\tilde{W}_2^T F_2^{-1}\dot{\tilde{W}}_2\right) \quad (40)$$

Using the estimated control signal $\hat{u}_1$ from RBFNN, Eq. (21) is rewritten as follows:

$$\dot{S} = \lambda_1 c_1 e_2 + \beta_1 c_2 e_4 + \lambda_1 f_1 + \beta_1 f_2 + (\lambda_1 g_1 + \beta_1 g_2)\hat{u}_1 - \lambda_1\ddot{x}_d - \beta_1\ddot{\theta}_d \quad (41)$$

Substituting (32), (33), (34) and (35) into (41), one can find out that:

$$\dot{S} = -\left(\eta_2 sat(S) + k_2 S\right) + \lambda_1\tilde{W}_1^T h + \beta_1\tilde{W}_2^T h + \lambda_1\varepsilon_1 + \beta_1\varepsilon_2 \quad (42)$$

From this it can be deduced that:

$$\dot{V} = \begin{pmatrix} -S\eta_2 sat(S) + k_2 S^2 + S_2\left(\lambda_1\varepsilon_1 + \beta_1\varepsilon_2\right) + \\ tr\left(\tilde{W}_1^T F_1^{-1}\dot{\tilde{W}}_1\right) + tr\left(\tilde{W}_2^T F_2^{-1}\dot{\tilde{W}}_2\right) + \\ +S\lambda_1\tilde{W}_1^T h + S\beta_1\tilde{W}_2^T h \end{pmatrix}$$

$$\dot{V} = \begin{pmatrix} -S\eta_2 sat(S) + k_2 S^2 + S\left(\lambda_1\varepsilon_1 + \beta_1\varepsilon_2\right) + \\ tr\left\{\tilde{W}_1^T\left(S\lambda_1 h - F_1^{-1}\dot{\tilde{W}}_1\right)\right\} + tr\left\{\tilde{W}_2^T\left(S\beta_1 h - F_2^{-1}\dot{\tilde{W}}_2\right)\right\} \end{pmatrix} \quad (43)$$

Substituting (37) into (43), we obtain:

$$\dot{V} = \begin{pmatrix} -S\left(\eta_2 sat(S) + k_2 S\right) + S\left(\lambda_1\varepsilon_1 + \beta_1\varepsilon_2\right) \\ +\alpha\|S\|\left\{tr\left(\tilde{W}_1^T\left(W_1 - \tilde{W}_1\right)\right) + tr\left(\tilde{W}_2^T\left(W_2 - \tilde{W}_2\right)\right)\right\} \end{pmatrix} \quad (44)$$

Next, we consider the following Lyapunov function

$$V_3 = \frac{1}{2}s_3^2 + \frac{1}{2}tr\left(\tilde{W}_3^T F_3^{-1}\tilde{W}_3\right) \quad (45)$$

Taking the time derivative of V_3 gives

$$\dot{V}_3 = s_3\dot{s}_3 + tr\left(\tilde{W}_3^T F_3^{-1}\dot{\tilde{W}}_3\right) \quad (46)$$

Eq. (27) gives us:

$$\dot{V}_3 = s_3\left(g_3\hat{u}_2 + f_3 - \ddot{\psi}_d + c_3 e_6\right) + tr\left(\tilde{W}_3^T F_3^{-1}\dot{\tilde{W}}_3\right) \quad (47)$$

Substituting (36) into (47) results in:

$$\begin{aligned} \dot{V}_3 &= -s_3\left(k_3 sat(s_3) + \eta_3 s_3\right) + s_3\left(f_3 - \hat{f}_3\right) + tr\left(\tilde{W}_3^T F_3^{-1}\dot{\tilde{W}}_3\right) \\ &= -s_3\left(k_3 sat(s_3) + \eta_3 s_3\right) + s_3\left(W_3^T h + \varepsilon_3 - \hat{W}_3^T h\right) + tr\left(\tilde{W}_3^T F_3^{-1}\dot{\tilde{W}}_3\right) \\ &= -s_3 k_3 sat(s_3) - \eta_3 s_3^2 + s\varepsilon_3 + s_3\tilde{W}_3^T h + tr\left(\tilde{W}_3^T F_3^{-1}\dot{\tilde{W}}_3\right) \\ &= -s_3 k_3 sat(s_3) - \eta_3 s_3^2 + s_3\varepsilon_3 + tr\left(\tilde{W}_3^T\left(s_3 h - F_3^{-1}\dot{\tilde{W}}_3\right)\right) \end{aligned} \quad (48)$$

Substituting (37) into (48) gives

$$\dot{V}_3 = -s_3 k_3 sat(s_3) - \eta_3 s_3^2 + s_3\varepsilon_3 + \sigma\|s_3\|tr\left(\tilde{W}_3^T\left(W_3 - \tilde{W}_3\right)\right) \quad (49)$$

Notice that $tr\left(\tilde{W}_3^T\tilde{W}_3\right) = \|\tilde{W}_3\|_F^2$.

Using the Cauchy-Schwart inequality, we have

$$tr\left(\tilde{W}_i^T\left(W_i - \tilde{W}_i\right)\right) \le \|W_i\|_F\|\tilde{W}_i\|_F - \|\tilde{W}_i\|_F^2, i = 1, 2, 3$$

It can be deduced from (44), (49) that

$$\dot{V} \le \begin{cases} -S\eta_2 sat(S) - k_2 S^2 + S\left(\lambda_1\varepsilon_1 + \beta_1\varepsilon_2\right) \\ +\alpha\|S\|\left(\|\tilde{W}_1\|_F\|W_1\|_F - \|\tilde{W}_1\|_F^2\right) + \alpha\|S\|\left(\|\tilde{W}_2\|_F\|W_2\|_F - \|\tilde{W}_2\|_F^2\right) \end{cases} \quad (50)$$

$$\dot{V}_3 \le -s_3 k_3 sat(s_3) - \eta_3 s_3^2 + s_3\varepsilon_3 + \sigma\|s_3\|\left(\|\tilde{W}_3\|_F\|W_3\|_F - \|\tilde{W}_3\|_F^2\right) \quad (51)$$

Hence

$$\dot{V} \le \begin{cases} -S\eta_2 sat(S) - \alpha\|S\|\left(\|\tilde{W}_1\|_F - \frac{1}{2}\|W_1\|_F\right)^2 - \alpha\|S\|\left(\|\tilde{W}_2\|_F - \frac{1}{2}\|W_2\|_F\right)^2 - \\ -\|S\|\left(k_2\|S\| - \varepsilon_{N1} - \alpha\frac{\|\tilde{W}_1\|_F^2 + \|\tilde{W}_2\|_F^2}{4}\right) \end{cases} \quad (52)$$

$$\dot{V}_3 \le -s_3 k_3 sat(s_3) - \sigma\|s_3\|\left(\|\tilde{W}_3\|_F - \frac{1}{2}\|W_3\|_F\right)^2 - \|s_3\|\left(\eta_3\|s_3\| - \varepsilon_{N2} - \sigma\frac{\|\tilde{W}_3\|_F^2}{4}\right)$$

Thus, if condition (38) is satisfied, one can deduce that:

$$\begin{cases} k_2\|S\| - \varepsilon_{N1} - \alpha\dfrac{\|\tilde{W}_1\|_F^2 + \|\tilde{W}_2\|_F^2}{4} > 0 \\ \eta_3\|s_3\| - \varepsilon_{N2} - \sigma\dfrac{\|\tilde{W}_3\|_F^2}{4} > 0 \end{cases} \Rightarrow \begin{cases} \dot{V} < 0 \\ \dot{V}_3 < 0 \end{cases}$$

This means that all subsystems in (5) are asymptotically stable at the origin by Lyapunov's criteria. The theorem has been proved.

4. SIMULATION RESULTS

To verify the effectiveness of the AFHSMC controller, we conducted some simulations using Matlab software. As a comparison of both controllers, simulations were also performed with the HSMC controller.

For the simulations, the TWSBMR system parameters are assumed to be known as

m_b = 116(kg), J = 16.25(kg.m^2), r = 0.1(m), l = 0.23(m), I_1 = 0.26(kg.m^2), d = 0.19(m), m_w = 11.4(kg), I_2 = 0.165 (kg.m^2), I_3 = 0.2(kg.m^2), b_y = 5(Ns.m), b_{rx} = 3.68 (Ns.m), g = 10(m/s^2), α = 56°

In addition, the controller parameters are determined empirically, i.e., error and trial, to achieve the best possible control quality.

$λ_1$ = 3, $β_1$ = 0.1, c_1 = 5, c_2 = 0.01, k_2 = 0.01, $η_2$ = 10, λ = 12, k_3 = 3, $η_3$ = 2, l = 15, F_1 = F_2 = 5, F_3 = 20, α = 0.1, σ = 0.65

We verified the system's responses using the following reference values: x_d = 1(m), $θ_d$ = 0(degree), $ψ_d$ = (180/π)x0.1sin(2πt) (degree)

We invested two experiments in a simulated environment with/without the effect of unknown external disturbances.

(a) Straight motion

(b) Pitch motion
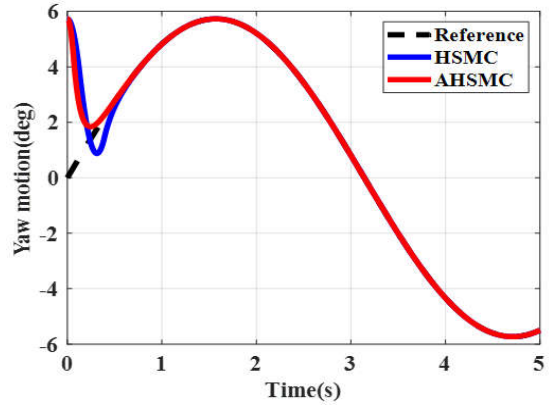
(c) Yaw motion

Figure 4. Simulation results without unknown external disturbance

Figure 4 shows the system's responses in the absence of external disturbances. For both AFHSMC and HSMC controllers, all responses rapidly approached and stabilized at their reference values. These results show that AFHSMC's control quality is better than HSMC's, especially with regard to pitch and yaw motions.

Figure 5 shows that AFHSMC outperforms HSMC under external disturbances. In the case of TWSBMR systems equipped with the HSMC controller, all system outputs are knocked out of steady equilibrium as soon as external noise appears. Meanwhile, with the AFHSMC controller, all system outputs are almost unaffected by external noises. These results are because the AFHSMC controller has strong adaptability to the model uncertainty and the effects of unknown external disturbances with the proposed adaptive law.
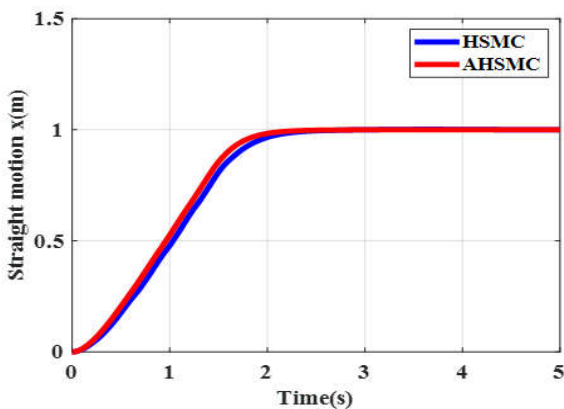
(a) Straight motion
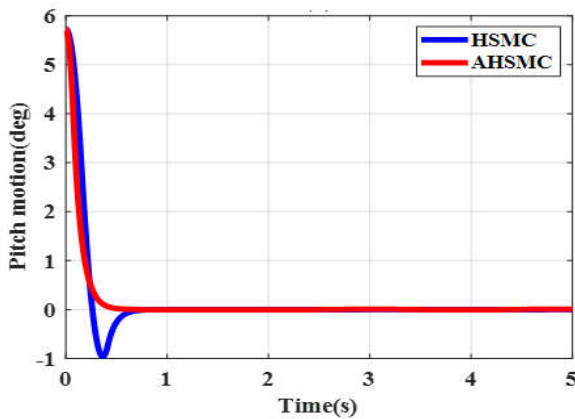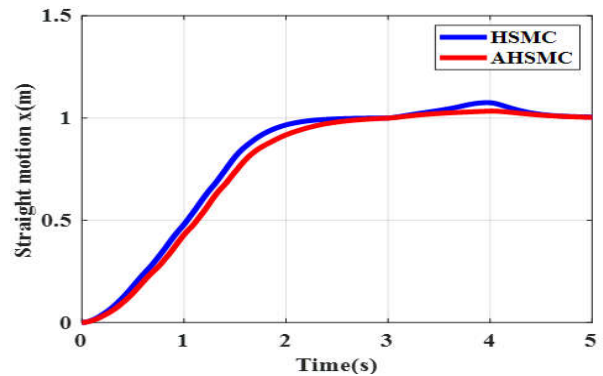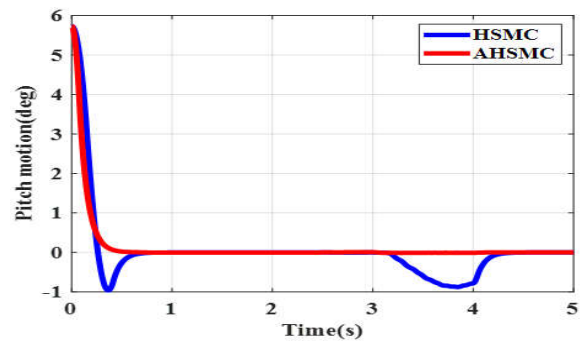
(b) Pitch motion

(c) Yaw motion
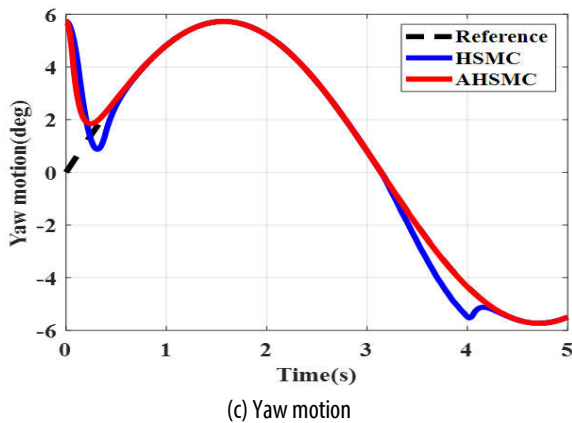
Figure 5. Simulation results with unknown external disturbance

Thus, the simulation results demonstrate that the proposed controller can accurately control the position and orientation of the TWSBMR while maintaining a minimal pitch angle. Furthermore, the proposed controller is robust against external noise as the TWSBMR moves.

5. CONCLUSION

This paper has proposed an adaptive controller for TWSBMR combining SMC, hierarchical SMC (HSMC) and RBF neural network. The controller SMC-HSMC acts as the central controller to ensure the stable system's state on the sliding surface. An adaptive rule is designed to approximate the uncertain components in the system. Consequently, the proposed controller is robust in actual TWSBMR control under uncertain model parameters or unexpected external disturbances. The simulation results show that the system responses quickly converge to their reference and are little affected by unknown external disturbances. The stability of the proposed control system is also rigorously proven according to Lyapunov's principle. In the subsequent studies, we will test the proposed algorithm for actual TWSBMR and verify the effectiveness of the proposed controller with many real-life scenarios.

REFERENCES

[1]. Y.S. Ha, S. i. Yuta, 1996. *Trajectory tracking control for navigation of the inverse pendulum type self-contained mobile robot.* Robotics Auton. Syst., vol. 17, pp. 65-80.

[2]. F. Grasser, A. D'Arrigo, S. Colombi, A. C. Rufer, 2002. *JOE: a mobile, inverted pendulum*. IEEE Trans. Ind. Electron., vol. 49, pp. 107-114.

[3]. T. Takei, R. Imamura, S. i. Yuta, 2009. *Baggage Transportation and Navigation by a Wheeled Inverted Pendulum Mobile Robot.* IEEE Transactions on Industrial Electronics, vol. 56, pp. 3985-3994.

[4]. S. C. Lin, C. C. Tsai, H. C. Huang, 2011. *Adaptive Robust Self-Balancing and Steering of a Two-Wheeled Human Transportation Vehicle.* Journal of Intelligent & Robotic Systems, vol. 62, pp. 103-123.

[5]. P. Petrov, M. Parent, 2010. *Dynamic modeling and adaptive motion control of a two-wheeled self-balancing vehicle for personal transport.* 13th International IEEE Conference on Intelligent Transportation Systems, pp. 1013-1018.

[6]. M. Stilman, J. Wang, K. Teeyapan, R. Marceau, 2009. *Optimized control strategies for wheeled humanoids and mobile manipulators.* 2009 9th IEEE-RAS International Conference on Humanoid Robots, pp. 568-573.

[7]. H. Uustal, J. L. Minkel, 2004. *Study of the Independence IBOT 3000 Mobility System: an innovative power mobility device, during use in community environments*. Archives of physical medicine and rehabilitation, vol. 85 12, pp. 2002-10.

[8]. M. Nikpour, L. Huang, A. M. Al-Jumaily, 2020. *Stability and Direction Control of a Two-Wheeled Robotic Wheelchair Through a Movable Mechanism*. IEEE Access, vol. 8, pp. 45221-45230.

[9]. R. P. M. Chan, K. A. Stol, R. Halkyard, 2013. *Review of modelling and control of two-wheeled robots.* Annu. Rev. Control., vol. 37, pp. 89-103.

[10]. J. Meng, A. Liu, Y. Yang, Z. Wu, Q. Xu, 2018. *Two-Wheeled Robot Platform Based on PID Control.* in 2018 5th International Conference on Information Science and Control Engineering (ICISCE), pp. 1011-1014.

[11]. V. Mudeng, B. Hassanah, Y. T. K. Priyanto, O. Saputra, 2020. *Design and Simulation of Two-Wheeled Balancing Mobile Robot with PID Controller*. International Journal of Sustainable Transportation Technology, Volume 3, Issue 1, pp 12-19

[12]. C. Ben Jabeur, H. Seddik, 2020. *Design of a PID optimized neural networks and PD fuzzy logic controllers for a two wheeled mobile robot.* Asian Journal of Control.

[13]. A. Fahmi, et al., 2020. *Modelling and Control using Pole Placement Method for Self Balancing Robot.* Solid State Technology, vol. 63, pp. 1314-1324.

[14]. Y. Amano, 2014. *Stability Control for Two-Wheeled Mobile Robot Using Robust Pole-Placement Method.*

[15]. N. Uddin, T. A. Nugroho, W. A. Pramudito, 2017. *Stabilizing Two-wheeled robot using linear quadratic regulator and states estimation.* 2017 2nd International conferences on Information Technology, Information Systems and Electrical Engineering (ICITISEE), pp. 229-234.

[16]. P. Oryschuk, A. Salerno, A. M. Al-Husseini, J. Angeles, 2009. *Experimental Validation of an Underactuated Two-Wheeled Mobile Robot.* IEEE/ASME Transactions on Mechatronics, vol. 14, pp. 252-257.

[17]. S. Kim, S. Kwon, 2017. *Nonlinear Optimal Control Design for Underactuated Two-Wheeled Inverted Pendulum Mobile Platform*. IEEE/ASME Transactions on Mechatronics, vol. 22, pp. 2803-2808.

[18]. K. Pathak, J. Franch, S. K. Agrawal, 2005. *Velocity and position control of a wheeled inverted pendulum by partial feedback linearization.* IEEE Transactions on Robotics, vol. 21, pp. 505-513.

[19]. M. Muhammad, S. Buyamin, M. N. Ahmad, S. W. Nawawi, Z. Ibrahim, 2012. *Velocity tracking control of a Two-Wheeled Inverted Pendulum robot: A comparative assessment between partial feedback linearization and LQR control schemes.* International Review on Modelling and Simulations, vol. 5, pp. 1038-1048.

[20]. M. Önkol, C. k. Kasnakp lu, 2018. *Adaptive Model Predictive Control of a Two-wheeled Robot Manipulator with Varying Mass.* Measurement and Control, vol. 51, pp. 38 - 56.

[21]. D. P. Nam, N. H. Quang, D. C. H. Phi, T. N. Anh, D. Bao, 2019. *Robust Model Predictive Control Based Kinematic Controller for Nonholonomic Wheeled Mobile Robotic Systems*. Lecture Notes in Networks and Systems Springer International Publishing.

[22]. A. Sinha, P. Prasoon, P. Bharadwaj, A. Ranasinghe, 2015. *Nonlinear Autonomous Control of a Two-Wheeled Inverted Pendulum Mobile Robot Based on*

Sliding Mode. 2015 International Conference on Computational Intelligence and Networks, pp. 52-57.

[23]. N. Esmaeili, A. Alfi, H. Khosravi, 2017. *Balancing and Trajectory Tracking of Two-Wheeled Mobile Robot Using Backstepping Sliding Mode Control: Design and Experiments.* Journal of Intelligent & Robotic Systems, vol. 87, pp. 601-613.

[24]. J. Mu, X. g. Yan, S. K. Spurgeon, Z. Mao, 2017. *Nonlinear sliding mode control of a two-wheeled mobile robot system.* Int. J. Model. Identif. Control., vol. 27, pp. 75-83.

[25]. M. Begnini, D. W. Bertol, N. A. Martins, 2017. *A robust adaptive fuzzy variable structure tracking control for the wheeled mobile robot: Simulation and experimental results.* Control Engineering Practice, vol. 64, pp. 27-43.

[26]. G. R. Yu, Y. K. Leu, H. T. Huang, 2017. *PSO-based fuzzy control of a self-balancing two-wheeled robot.* 2017 Joint 17th World Congress of International Fuzzy Systems Association and 9th International Conference on Soft Computing and Intelligent Systems (IFSA-SCIS), pp. 1-5.

[27]. Á. Odry, I. Kecskés, E. Burkus, P. Odry, 2017. *Protective Fuzzy Control of a Two-Wheeled Mobile Pendulum Robot: Design and Optimization.* WSEAS Transactions on Systems and Control archive, vol. 12.

[28]. T. Zhao, Q. Yu, S. Dian, R. Guo, S. Li, 2019. *Non-singleton General Type-2 Fuzzy Control for a Two-Wheeled Self-Balancing Robot.* International Journal of Fuzzy Systems, pp. 1-14.

[29]. M. Muhammad, A. A. Bature, U. Zangina, S. Buyamin, A. Ahmad, M. A. Shamsudin, 2019. *Velocity control of a two-wheeled inverted pendulum mobile robot: a fuzzy model-based approach.* Bulletin of Electrical Engineering and Informatics.

[30]. C. C. Tsai, H. C. Huang, S. C. Lin, 2010. *Adaptive Neural Network Control of a Self-Balancing Two-Wheeled Scooter.* IEEE Transactions on Industrial Electronics, vol. 57, pp. 1420-1428.

[31]. A. I. Glushchenko, V. A. Petrov, K. A. Lastochkin, 2018. *On Development of Neural Network Controller with Online Training to Control Two-Wheeled Balancing Robot.* 2018 International Russian Automation Conference (RusAutoCon), pp. 1-6.

[32]. A. Chhotray, D. R. Parhi, 2019. *Navigational Control Analysis of Two-Wheeled Self-Balancing Robot in an Unknown Terrain Using Back-Propagation Neural Network Integrated Modified DAYANI Approach.* Robotica, vol. 37, pp. 1346 - 1362.

[33]. A. Maity, S. Bhargava, 2020. *Design and Implementation of a Self-Balancing Two-Wheeled Robot Driven by a Feed-Forward Backpropagation Neural Network.* IRJET Journal Volume 7, Issue 9.

[34]. A. Filipescu, V. Mînzu, B. Dumitrascu, A. Filipescu, E. Minca, 2011. *Trajectory-tracking and discrete-time sliding-mode control of wheeled mobile robots.* 2011 IEEE International Conference on Information and Automation, pp. 27-32.

[35]. P. N. Mali, N. G. Kulkarni, 2015. Discrete-Time Sliding Mode Control for Wheeled Mobile Robot Trajectory-Tracking. IOSR Journal of Electrical and Electronics Engineering (IOSR-JEEE) Volume 10, Issue 3 Ver. III.

[36]. H. Aithal, S. Janardhanan, 2013. *Trajectory tracking of two wheeled mobile robot using higher order sliding mode control.* 2013 International Conference on Control, Computing, Communication and Materials (ICCCCM), pp. 1-4.

[37]. D. Qian, J. Yi, D. Zhao, 2008. *Hierarchical sliding mode control for a class of SIMO under-actuated systems.* Control and Cybernetics, vol. 37, pp. 159-175.

[38]. J. Liu, 2017. *Intelligent Control Design and MATLAB Simulation.* Springer.

[39]. S. Kim, S. Kwon, 2015. *Dynamic modeling of a two-wheeled inverted pendulum balancing mobile robot.* International Journal of Control, Automation and Systems, vol. 13, pp. 926-933.

THÔNG TIN TÁC GIẢ

Hoàng Thị Tú Uyên[1], Kim Đình Thái[2], Phạm Việt Anh[2], Đinh Xuân Minh[3], Lê Xuân Hải[2]

[1]Khoa Tự động hóa, Trường Đại học Công nghiệp Thành phố Hồ Chí Minh

[2]Viện Công nghệ HaUI, Trường Đại học Công nghiệp Hà Nội

[3]Khoa Điện tử, Trường Đại học Công nghiệp Hà Nội